Molecular Pharmacology Fast Forward. Published on October 2, 2020 as DOI: 10.1124/molpharm.120.000104
This article has not been copyedited and formatted. The final version may differ from this version.

MOLPHARM-AR-2020-000104

Arginine-259 of UDP-glycosyltransferase 2B7 (UGT2B7) confers UDP-sugar selectivity

Pramod C. Nair[1,2#], Nuy Chau[1#], Ross A. McKinnon[2] and John O. Miners[1,2]

[1]Department of Clinical Pharmacology, Flinders University College of Medicine and Public Health, Flinders Medical Centre, Bedford Park, SA 5042, Australia.

[2] FHMRI Cancer Program, Flinders Health and Medical Research Institute, Flinders University College of Medicine and Public Health, Flinders Medical Centre, Bedford Park, SA 5042, Australia.

#Joint first authors.

Downloaded from molpharm.aspetjournals.org at ASPET Journals on April 19, 2024

Molecular Pharmacology Fast Forward. Published on October 2, 2020 as DOI: 10.1124/molpharm.120.000104
This article has not been copyedited and formatted. The final version may differ from this version.

MOLPHARM-AR-2020-000104

Running title: Arginine-259 of UGT2B7 confers UDP-sugar selectivity

Corresponding author: Dr Pramod C. Nair,

Department of Clinical Pharmacology,

College of Medicine and Public Health,

Flinders University,

GPO Box 2100, Adelaide, SA 5001,

Australia.

Email pramod.nair@flinders.edu.au;

telephone 61-8-82043155; fax 61-8-82045114.

Text pages: 30

Number of figures: 4

Number of supplemental table(s): 1

Number of supplemental figure(s): 3

Number of supplemental MPEG movie: 1

Number of references: 43

Abstract: 195 words

Introduction: 808 words

Results: 1726 words

Discussion: 1429 words

Abbreviations: MD, molecular dynamics; UGT, (UDP)-glycosyltransferase; UDP-GlcUA, UDP-glucuronic acid; UDP-Glc UDP-glucose; 4MU, 4-Methylumbelliferone; AZT, zidovudine.

Downloaded from molpharm.aspetjournals.org at ASPET Journals on April 19, 2024

Molecular Pharmacology Fast Forward. Published on October 2, 2020 as DOI: 10.1124/molpharm.120.000104
This article has not been copyedited and formatted. The final version may differ from this version.

MOLPHARM-AR-2020-000104

Abstract

Enzymes of the human uridine diphosphate (UDP)-glycosyltransferase (UGT) superfamily typically catalyse the covalent addition of the sugar moiety from a UDP-sugar cofactor to relatively low molecular weight lipophilic compounds. Although UDP-glucuronic acid (UDP-GlcUA) is most commonly employed as the cofactor by UGT1 and UGT2 family enzymes, UGT2B7 and several other enzymes can utilise both UDP-GlcUA and UDP-glucose (UDP-Glc), leading to the formation of glucuronide and glucoside conjugates. An investigation of UGT2B7 catalysed morphine glycosidation indicated that glucuronidation is the principal route of metabolism because the binding affinity of UDP-GlcUA is higher than that of UDP-Glc. Currently, it is unclear which residues in the UGT2B7 cofactor binding domain are responsible for the preferential binding of UDP-GlcUA. Here, molecular dynamics (MD) simulations were performed together with site-directed mutagenesis and enzyme kinetic studies to identify residues within the UGT2B7 binding site responsible for the selective cofactor binding. MD simulations demonstrated that Arg259, located within the N-terminal domain, specifically interacts with UDP-GlcUA whereby the side-chain of Arg259 H-bonds and forms a salt-bridge with the carboxylate group of glucuronic acid. Consistent with the MD simulations, substitution of Arg259 with Leu resulted in the loss of morphine, 4-methylumbelliferone, and zidovudine glucuronidation activity, but morphine glucosidation was preserved.

Downloaded from molpharm.aspetjournals.org at ASPET Journals on April 19, 2024

Molecular Pharmacology Fast Forward. Published on October 2, 2020 as DOI: 10.1124/molpharm.120.000104
This article has not been copyedited and formatted. The final version may differ from this version.

Significance Statement

Despite the importance of uridine diphosphate glycosyltransferase (UGT) enzymes in drug and chemical metabolism, cofactor binding interactions are incompletely understood as is the molecular basis for preferential glucuronidation by UGT1 and UGT2 family enzymes. Using a UGT2B7 homology model, this study demonstrated that long timescale molecular dynamics (MD) simulations can be used to identify key binding interactions of a UGT protein with cofactors may provide a basis for the application of MD simulations to the elucidation of UGT–aglycone interactions.

Downloaded from molpharm.aspetjournals.org at ASPET Journals on April 19, 2024

Molecular Pharmacology Fast Forward. Published on October 2, 2020 as DOI: 10.1124/molpharm.120.000104
This article has not been copyedited and formatted. The final version may differ from this version.

Introduction

Enzymes of the human uridine diphosphate (UDP)-glycosyltransferase (UGT) superfamily catalyse the transfer of a hexose moiety from a UDP-sugar to a nucleophilic acceptor functional group present in structurally diverse compounds that include drugs, non-drug xenobiotics and endobiotics (Miners and Mackenzie, 1991; Miners et al., 2004; Meech et al., 2019; Mackenzie et al., 2005; Radominska-Pandya., 1999). This versatility of UGT arises from the existence of multiple forms of the enzyme that exhibit distinct, but frequently overlapping, substrate selectivities (Miners et al, 2010). The twenty-two functional human UGT genes identified to date are classified into four families; UGT1, UGT2, UGT3 and UGT8. Utilisation of UDP-sugars by human UGTs varies between families and enzymes. For example, UGT3A1 and UGT3A2, the only members of the UGT3 family, use N-acetylglucosamine and UDP-glucose (UDP-Glc) as the respective cofactors, while UGT8A1 utilises only UDP-galactose (Mackenzie et al., 2008; Meech et al., 2012 and 2015). By contrast, enzymes of the UGT1 and UGT2 families primarily utilise UDP-glucuronic acid (UDP-GlcUA) as the cofactor, although some enzymes in these families are also known to catalyse glycosidation reactions other than glucuronidation (Meech et al., 2012). Nevertheless, glucuronidation is the major metabolic pathway since, at least with UGT2B7, the affinity of UDP-GlcUA is higher than that of the alternate UDP-sugar (Chau et al., 2014 and references therein). These observations suggest that differences in cofactor binding are responsible for the differing UDP-sugar selectivities of UGT enzymes.

UGT2B7 is considered to be one of the most important enzymes involved in drug glucuronidation. This enzyme contributes to the glucuronidation of drugs from numerous therapeutic classes that include opioids (e.g. codeine, morphine, naloxone), anticancer drugs (e.g. epirubicin), non-steroidal anti-inflammatory agents (e.g. diclofenac, naproxen),

Downloaded from molpharm.aspetjournals.org at ASPET Journals on April 19, 2024

Molecular Pharmacology Fast Forward. Published on October 2, 2020 as DOI: 10.1124/molpharm.120.000104
This article has not been copyedited and formatted. The final version may differ from this version.

anticonvulsants (e.g. lamotrigine, valproic acid), antibiotics (e.g. chloramphenicol), and anti-retroviral agents (e.g. zidovudine; AZT) (Miners et al., 2010; Radominska-Pandya et al., 2001; Stingl et al, 2014). Morphine (3- and 6- glucuronidation) and AZT are the prototypic selective substrates of UGT2B7 (Court et al., 2003; Stone et al., 2003; Miners et al., 2010).

Of note, however, UGT2B7 also catalyses the glucosidation of several drugs, including the 3-glucosidation of morphine (Chau et al., 2014). The respective cofactors for glucosidation and glucuronidation reactions are UDP-Glc and UDP-GlcUA. UDP-glucose dehydrogenase catalyses the synthesis of UDP-GlcUA from UDP-Glc by a two stage NAD^+-dependent reaction (Feingold and Franzen 1981), and hence both cofactors are available in hepatocytes for drug and chemical conjugation. However, it remains unclear which residues within the UGT2B7 binding site contribute towards the higher binding affinity of UDP-GlcUA that favours glucuronidation over glucosidation.

The C-terminal (CT) domain is highly conserved across the human UGT family (Mackenzie et al., 2005; Radominska-Pandya et al, 1999). In particular, ~45 conserved residues, referred to the UGT signature sequence, located in the CT domain have been identified as a key region for UDP-sugar binding from sequence alignment, chimeragenesis and site-directed mutagenesis studies, and from the X-ray crystal structures of plant UGTs (Mackenzie et al., 2005; Meech et al., 2012, 2015; Offen et al. 2006). Although an X-ray crystal structure of a full-length mammalian UGT protein is unavailable, partial structures of the CT domain of human UGT2B7 and UGT2B15 without bound UDP-sugar have been published (Miley et al., 2007; Zhang et al., 2020). Taken together, the data demonstrate that the UDP-sugar and substrate (aglycone) binding domains occur predominantly in the CT and N-terminal (NT) domains, respectively (Miley et al., 2007; Nair et al., 2015). However, the partial X-ray

Downloaded from molpharm.aspetjournals.org at ASPET Journals on April 19, 2024

Molecular Pharmacology Fast Forward. Published on October 2, 2020 as DOI: 10.1124/molpharm.120.000104
This article has not been copyedited and formatted. The final version may differ from this version.

crystal structures and structure-function studies have only provided limited understanding into the UDP-sugar selectivity of human UGT enzymes. For instance, molecular modelling studies of the UGT2B7 protein identified CT domain residues (e.g. Asn378, Asn402) associated with preferential binding of UDP-GlcUA over UDP-Glc (Miley et al., 2007; Chau et al., 2014). However, mutagenesis of these amino acids led to loss of all glycosidation activity, inconsistent with a selective role in cofactor binding (Chau et al., 2014).

Homology models of several UGT enzymes have been developed in this laboratory to investigate the UDP-sugar selectivites of UGT 2 (including UGT2B7), 3 and 8 family proteins (Nair et al., 2015). Homology models of the CT domain showed a highly conserved structural fold with respect to the UGT2B7-CT X-ray crystal structure (root mean-squared deviations (rmsd) between 0.066 – 0.079 Å) and predicted interactions consistent with those anticipated from the X-ray crystal structure (Miley et al. 2007). Based on a full-length homology model of UGT2B7, we postulated that residue(s) from the NT domain are important in the for UDP-sugar recognition and may play a significant role in the cofactor selectivities of UGT enzymes. However, the static models provided limited insight into how individual residues and their flexibility contributed towards UDP-sugar binding and selectivity. In this study, we used long molecular dynamics simulation (MDS) times together with site-directed mutagenesis and enzyme activity assays to demonstrate that Arg-259 of the NT domain plays a pivotal role in the binding selectivity of UDP-GlcUA.

Materials and Methods

Chemicals and other reagents

4-Methylumbelliferone (4MU), 4-methylumbelliferone glucuronide (4MUG), morphine 3-β-D-glucuronide (M3G), morphine 6-β-D-glucuronide (M6G), 1-octanesulfonic acid sodium

Downloaded from molpharm.aspetjournals.org at ASPET Journals on April 19, 2024

Molecular Pharmacology Fast Forward. Published on October 2, 2020 as DOI: 10.1124/molpharm.120.000104
This article has not been copyedited and formatted. The final version may differ from this version.

salt, UDP-Glc; (disodium salt) from *Saccharomyces cerevisiae*, UDP-GlcUA (trisodium salt), puromycin, ammonium persulphate (APS), zidovudine (AZT) and zidovudine glucuronide (GAZT) were purchased from Sigma-Aldrich (Sydney, NSW, Australia). Phusion® High-Fidelity DNA Polymerase, 1kb DNA Ladder and restriction enzymes were from New England Biolabs (Ipswich, MA); Dulbecco's Modified Eagle Medium (DMEM), Lipofectamine^{TM} 2000, MEM non-essential amino acids, MEM sodium pyruvate, peptone, Opti-MEM PLUS reagent and Penicillin Streptomycin (Pen Strep) were from Invitrogen (Mount Waverley, Vic, Australia). Morphine hydrochloride was obtained from GlaxoSmithKline (Melbourne, Australia). Morphine 3-glucoside was synthesised in-house, as described by Chau et al. (2014). Solvents and other reagents including acetic acid, acetonitrile, triethylamine (TEA), and perchloric acid were of analytical reagent grade.

Comparative Modelling and Molecular Dynamics (MD) Simulations

A UGT2B7 homology model (residues 23-469) has been developed in this laboratory based on the X-ray crystal structure of *Medicago truncatula* UGT85H2 (PDB 2PQ6) using SWISS-MODEL (Nair et al., 2015). *In silico* mutants were generated by substituting Arg259 of the wild-type structure with Ala and Leu (see Results and Discussion) using the mutagenesis tool in PyMOL (PyMOL, Version 2.0 Schrödinger, LLC). MD simulations of the wild-type and mutant UGT2B7 proteins were performed using GROMACS 2019 in conjunction with the GROMOS 54A7 force field (Schmid et al., 2011; Abraham et al., 2015). The simple point charge (SPC) water model was used to describe the solvent water. Simulations were performed under periodic boundary conditions in a rectangular box. A cut-off of 1.4 nm was applied to short-range non-bonded interactions, whereas long-range electrostatic interactions were calculated using the particle mesh Ewald (PME) algorithm (Darden et al., 1993; Essmann et al., 1995). UDP-GlcUA and UGP-Glc were predicted to have charge states of -3

Downloaded from molpharm.aspetjournals.org at ASPET Journals on April 19, 2024

Molecular Pharmacology Fast Forward. Published on October 2, 2020 as DOI: 10.1124/molpharm.120.000104
This article has not been copyedited and formatted. The final version may differ from this version.

and -2, respectively, at pH 7.4, using the Calculator Plugins implemented in ChemAxon (Marvin 16.6.20). Topology parameters for UDP-GlcUA and UGP-Glc were obtained using the Automated Topology Builder and Repository (Malde et al., 2011).

UDP-GlcUA and UDP-Glc were docked into the cofactor binding domain by overlaying the template UDP-deoxy-fluoro-glucose from the VvGT1 crystal structure, as described previously (Meech et al., 2015; Nair et al., 2015). The UDP-Glc/UDP-GlcUA-UGT2B7 complexes were separately placed in a cubic box of SPC water, with neutralising counter ions. A steepest descents minimisation followed by a position restraint simulation for 250 ps was performed under a constant volume (NVT) ensemble. Constant pressure (NPT) equilibration was performed for 250 ps using weak coupling to maintain pressure isotropically at 1.0 bar at a temperature of 310°K. A Parrinello-Rahman barostat was used to isotropically regulate pressure along with a Nose´-Hoover thermostat to maintain temperature, ensuring that a true NPT ensemble is sampled (Parrinello and Rahman, 1981; Nosé, 1984; Hoover WG, 1985). Production MD simulations were conducted for 300 ns without any restraints. Simulations were performed for UGT2B7 wild-type and mutant (Arg259Ala and Arg259Leu) proteins with bound cofactor (UDP-GlcUA and UDP-Glc).

PCR-site-directed mutagenesis and expression of UGT2B7 proteins

The wild-type UGT2B7 cDNA in pBluescript II SK (+) was used as the template for site-directed mutagenesis (SDM). Primers employed for mutagenesis are shown in supplementary Table S1. PCR reactions, in a total volume of 50µL, contained 100ng of DNA template, 250ng of forward and reverse oligonucleotide primer, 0.2mM of each dNTP, and 1.0 U Phusion® High-Fidelity DNA Polymerase. Reaction mixtures were prepared in 5X Phusion® HF reaction buffer. The PCR reaction was performed using a RoboCycler Gradient 96

Downloaded from molpharm.aspetjournals.org at ASPET Journals on April 19, 2024

Molecular Pharmacology Fast Forward. Published on October 2, 2020 as DOI: 10.1124/molpharm.120.000104
This article has not been copyedited and formatted. The final version may differ from this version.

temperature cycler (Stratagene, La Jolla, CA). Cycling parameters were: 3min at 98°C for DNA denaturation and activation of the polymerase, followed by 18 cycles of 10sec at 98°C for denaturation, 1 min at 55°C for primer annealing and 14min at 68°C for extension, with a final extension of 15min at 68°C. PCR products were purified using the QIAquick PCR Purification Kit. The PCR product was then digested with 20U of *Dpn* I (37°C for 60min) to cleave the methylated template plasmid and heat inactivated at 80°C for 20min. After transformation into DH5α cells and purification, wild-type and mutant UGT2B7 coding sequences were then ligated into the mammalian vector pEF-IRES-puro 5 using the restriction enzymes *Xho*I and *Xba*I. All mutations were confirmed on both strands by DNA sequencing using an Applied Biosystems 3130xl Genetic Analyser with BigDye Terminator v3.1 Chemistry (Applied Biosystems, Foster City, CA). UGT2B7 and wild-type and mutant cDNAs were stably expressed in HEK293T cells following the procedure of Uchaipichat et al. (2004), as modified by Chau et al. (2014).

Immunoblotting

Cell lysate from HEK293T cells expressing wild-type and mutant UGT2B7 proteins (50µg) were separated by 10% SDS-polyacrylamide gel electrophoresis and transferred to nitrocellulose (0.45µm; Bio-Rad Laboratories, Inc., CA). Immunodetection of UGT2B7 proteins was performed by probing with rabbit anti-human UGT2B7 (polyclonal) primary antisera (Kerdpin et al., 2009) diluted 1:2000 followed by incubation with Peroxidase AffiniPure Donkey Anti-Rabbit IgG (H+L) secondary HRP-conjugated IgG (Jackson ImmunoResearch Laboratories, Inc., PA, USA) diluted 1:4000. Immunoreactivity was detected using the Clarity™ Western ECL Substrate (Bio-Rad Laboratories, Inc., CA). Blots were visualised with a Fujifilm LAS-4000 imaging system (Fujifilm Life Sciences, NSW, Australia) and band intensities were measured using Image Studio™ Lite Version 5.2 (LI-

Downloaded from molpharm.aspetjournals.org at ASPET Journals on April 19, 2024

Molecular Pharmacology Fast Forward. Published on October 2, 2020 as DOI: 10.1124/molpharm.120.000104
This article has not been copyedited and formatted. The final version may differ from this version.

COR, Inc., Nebraska). Relative UGT2B7 protein levels represent the mean of quadruplicate measurements. Western blot analysis and activity assays were performed using the same batch of cell lysate.

Morphine 3- and 6-glycosidation, AZT and 4MU glucuronidation assays and metabolite quantification

The method employed was a modification of the procedure for morphine 3- and 6-glucuronidation reported by Uchaipichat et al. (2011). Briefly, incubations, in a total volume of 200µL, contained phosphate buffer (0.1M, pH 7.4), $MgCl_2$ (4mM), recombinant UGTs expressed in HEK293 cells (0.4mg), morphine (1-10mM) and UDP-GlcUA or UDP-Glc (5mM). After a 5min pre-incubation at 37˚C in a shaking water bath, reactions were initiated by the addition of cofactor (UDP-Glc or UDP-GlcUA) and performed for 150min. Reactions were terminated by the addition of perchloric acid (11.6M; 2µL) and cooling on ice for 10min. Samples were centrifuged (5000*g* for 10min), and a 10µL aliquot of the supernatant fraction was analysed by HPLC.

Experiments utilising AZT and 4MU as the aglycones and UDP-GlcUA as the cofactor were as described for the morphine glycosidation assay, except for altered protein concentration (0.3mg and 0.2mg of HEK293 cell lysate, respectively) and incubation time (60min) (Lewis et al, 2007; Rowland et al, 2007). The respective concentrations of AZT and 4MU in incubations ranged from 0.1-1mM and 0.05-0.7mM, respectively. Reactions were terminated with 2µL of perchloric acid and an aliquot (15µL and 40µL, respectively) of the supernatant fraction was analysed by HPLC. M3G, M6G, morphine 3-glucoside and 4-MUG formation was quantified by HPLC as described by Chau et al. (2014), while GAZT formation was measured according to Rowland et al. (2007) and Lewis et al. (2007).

Downloaded from molpharm.aspetjournals.org at ASPET Journals on April 19, 2024

Molecular Pharmacology Fast Forward. Published on October 2, 2020 as DOI: 10.1124/molpharm.120.000104
This article has not been copyedited and formatted. The final version may differ from this version.

Results

UGT2B7 Homology model and MDS

A human UGT2B7 homology model was constructed using the X-ray crystal structure of UGT85H2 from *Medicago truncatula*. The model incorporates a GT-B fold that distinguishes the CT and NT domains (Figure 1A), consistent with previously published plant UGT X-ray crystal structures. Similar to the UGT2B7-CT X-ray crystal structure, the CT domain of the model includes a highly conserved secondary structure with a Rossman-type fold, where seven α-helices envelope a single parallel β-sheet comprising six individual strands with a rmsd of 1.6 Å. The signature sequence (residues 356-399) of the CT domain, which is associated with UDP-sugar binding, is shown in Figure 1B. Like the previous full-length UGT2B7 model developed by Miley et al. (2007), Ser34, His35, and Asp151 are located in close proximity to the signature sequence; for example, the distance between Ser34 and Asn378 is 3.2 Å. These residues are thought to function as a serine hydrolase-like catalytic triad (Miley et al., 2007).

NT domain amino acids contribute to UDP-sugar binding and confer UDP-sugar selectivity

MD simulations of the UDP-Glc and UDP-GlcUA bound structures showed Tyr33 and Met37 are located within 5 Å of the uracil moiety of the UDP-sugar (Figure 2A and 2B). It has been demonstrated that the S atom of methionine (Met) can interact with aromatic (Aro) amino acids. The so-called Met-Aro interactions are generally stronger than hydrophobic interactions, resulting in additional stabilisation of 1–1.5 kcal/mol (Valley et al. 2012). It has also been demonstrated that Met can participate in Aro-Met-Aro bridging interactions, which are highly stabilising and can serve as ‘recognition’ motifs (Weber and Warren 2019). During

Downloaded from molpharm.aspetjournals.org at ASPET Journals on April 19, 2024

Molecular Pharmacology Fast Forward. Published on October 2, 2020 as DOI: 10.1124/molpharm.120.000104
This article has not been copyedited and formatted. The final version may differ from this version.

the simulations of unliganded UGT2B7 it was observed that Tyr33 and Trp356 are located within 5 Å of Met37, and this results in a Tyr33-Met37-Trp356 bridging interaction. Simulations of UGT2B7 in the presence of UDP-Glc and UDP-GlcUA showed two additional bridging interactions involving the uracil ring of the UDP-sugar (viz. Tyr33-Met37-uracil and Trp356-Met37-uracil). In addition, there is an edge-to-face aromatic pi-pi interaction between Tyr33 and the uracil ring of the UDP-sugar. Furthermore, the Ser34 side-chain is flexible and H-bonds with the α-phosphate O2 atom. Simulations show a combination of hydrophobic, polar and aromatic residues (Ser173, Phe174 and Thr179) positioned within 5 Å of the sugar moiety of both UDP-Glc and UDP-GlcUA, which provides a binding pocket for the polar hydroxyl and hydrophobic -CH groups of the sugar rings.

A notable difference observed in the MD simulations of the UDP-Glc and UDP-GlcUA bound UGT2B7 complexes was the side-chain conformation of Arg259. In the simulations with UDP-Glc, the Arg259 side-chain spontaneously ‘flipped’ away from the UDP-sugar binding site such that the distance between the O atom of the -CH_2OH group of UDP-Glc and the -NH of the guanidinium moiety of arginine equilibrated at a distance of approximately 12 Å (Figure 3A). While the simulations showed that the side-chain -CH_2OH group of glucose is highly flexible and forms transient H-bonds with Ser173, Ser175, Thr179 and Ala377 (backbone -NH atom), H-bonding with Arg259 did not occur during the course of the simulation. In contrast, MD simulations of UDP-GlcUA bound UGT2B7 demonstrated a conformational ‘locking’ of the Arg259 side-chain and the carboxylate group of glucuronic acid. As shown in Figure 3B, the distance between the side-chain Arg259 and the carboxylate group fluctuates between the ‘in’ and ‘out’ conformations for the first 100ns of the simulation, but beyond 100ns the Arg259 side-chain remains in a stable locked conformation

Downloaded from molpharm.aspetjournals.org at ASPET Journals on April 19, 2024

Molecular Pharmacology Fast Forward. Published on October 2, 2020 as DOI: 10.1124/molpharm.120.000104
This article has not been copyedited and formatted. The final version may differ from this version.

such that the distance between the H atom of Arg259 (guanidinium group) and the carboxylate O atoms is relatively stable at approximately 2.2 Å (Supplementary Movie). In this orientation, the Arg259 side-chain also H-bonds with the side-chain of Asn378, which stabilises the locked conformation. In the locked orientation, a stable salt-bridge forms between the positively charged N atom of the guanidinium group of Arg259 and the negatively charged carboxylate O atom of glucuronic acid (Figure 3C); at equilibrium (>100ns), the distance between the two groups is approximately 3.8 Å.

UDP-Glc/UDP-GlcUA binding site at the CT domain

UGT2B7-UDP-Glc and UGT2B7-UDP-GlcUA complexes were obtained by docking the cofactors at the binding site near the signature sequence of the CT domain, as described previously (Nair et al., 2015; Meech et al., 2015). MD simulations of both complexes showed a stable binding mode within the cofactor binding domain, consistent with the previously identified site predicted by: the partial X-ray structure of UGT2B7; the plant X-ray crystal structures; and the homology models based on plant UGT templates (Offen et al., 2006; Miley et al., 2007, Nair et al., 2015).

In particular, simulations of UGT2B7 with bound UDP-Glc indicated a T-shaped aromatic ring stacking pi-pi interaction between the side-chain of Trp356 and the uracil of UDP-Glc, as predicted for human UGT2B7 and other UGT enzymes (Nair et al. 2015) (Figure 2A). Further, the uracil ring was found to lie in close proximity to Arg338, such that flexibility in the side chain allows H-bonding with O1 of the uracil ring. Tyr354, Ile357, Pro358 and Phe371 together form an aromatic hydrophobic ‘pocket’ near the uracil ring. The simulations also demonstrated H-bonding interactions (~2.5 Å) between the O atom of the ribose 1’-OH and the side-chain -NH of Gln359, whereas the carboxylate group of the Glu382 side-chain

Downloaded from molpharm.aspetjournals.org at ASPET Journals on April 19, 2024

Molecular Pharmacology Fast Forward. Published on October 2, 2020 as DOI: 10.1124/molpharm.120.000104
This article has not been copyedited and formatted. The final version may differ from this version.

formed an H-bond (~2 Å) with the 2'-OH group. Likewise, the side-chain hydroxyl of Thr373 and nitrogen ($N\varepsilon^2$) of His374 H-bond with the O1 atoms of α- and β- phosphate. Furthermore, the O2 atoms of α- and β-phosphate H-bonds with Ser311 (both side-chain and backbone atoms) and the backbone atoms of Asn378. The backbone -NH of Gly379 H-bonds with the O2 atom of the β-phosphate group. MD simulations of UDP-Glc at the UGT2B7 binding site further show an identical H-bonding pattern between Asp398 and Gln399 and the O atoms of the glucose ring, as predicted previously for UDP-GlcUA (Miley et al., 2007), and H-bonding interactions between the side chain -NH of Asn402 and the 3'OH/4'OH groups of the glucose ring. The residues at positions 398, 399 and 402 lie on the Cα5 helix of the CT domain. Simulations of the unliganded and the cofactor bound UGT2B7 show that the Cα5 helix region is relatively rigid compared to the loop region associated with residues (e.g. Arg338, Trp356, Ile357) that interact with the uracil ring of the UDP-sugar. This less malleable region of the CT domain may be an essential recognition site for the UDP-sugars as mutation of Asp398, Gln399 and Asn402 completely abolish glycosidation activity (Miley et al., 2007; Chau et al., 2014).

As alluded to above, MD simulations of UDP-GlcUA bound to UGT2B7 show similar interactions between the uracil ring and Arg338, Trp356, Leu357 to those noted for UDP-Glc (Fig 1B). Several of the differences observed in the MD simulations of UDP-GlcUA are associated with the positioning of side-chain atoms of some residues located near the ribose ring, phosphate groups, and glucuronic acid moiety. Specifically, Glu382 forms a bidentate H-bond with both -OH groups of ribose (~2 Å), whereas Gln359 moderately H-bonds (~3 Å) with the O atoms of the 1'-OH group. His374 repositions to H-bond with the O1 atom of β-phosphate and 2'OH/3'OH of glucuronic acid, whereas Gln399 H-bonds with 3'OH/4'OH glucuronic acid. The glucuronic acid moiety positions such that Asp398 makes electrostatic

Downloaded from molpharm.aspetjournals.org at ASPET Journals on April 19, 2024

Molecular Pharmacology Fast Forward. Published on October 2, 2020 as DOI: 10.1124/molpharm.120.000104
This article has not been copyedited and formatted. The final version may differ from this version.

contact with 4'OH instead of H-bonding as observed in the UDP-Glc simulations. This repositioning of the sugar ring is most likely due to the electrostatic repulsion between the carboxylate groups.

Site-directed mutagenesis confirms Arg259 as an important residue for the selective binding of UDP-GlcUA

To verify the importance of H-bond and salt-bridge formation between Arg259 and the carboxylate group of glucuronic acid in cofactor binding and selectivity, two mutants were generated; Arg259Leu and Arg259Ala. Leu has a neutral hydrophobic side-chain but similar volume to Arg, and substitution with Ala is a common approach for investigating the importance a residue in ligand binding. Wild-type UGT2B7 and the Arg259Ala and Arg259Leu mutants were stably expressed in HEK293T cells. Analysis of the densitometry data from quadruplicate blots provided mean (± SD) relative densities (compared to wild-type UGT2B7) of 0.16 ± 0.03 (Arg259Ala) and 0.39 ± 0.04 (Arg259Leu) (Supplementary S3). Human liver microsomes were used as the positive control while untransfected HEK293 lysate served as the negative control. Activities of UGT2B7 and the Arg259Ala and Arg259Leu mutants were determined for AZT, 4-MU and morphine with both UDP-Glc and UDP-GlcUA (5 mM) as the cofactors (Figure 4A-E). Activities, normalised for relative expression, were determined at 3 substrate (aglycone) concentrations that spanned the known K_m values for AZT, 4-MU and morphine glucuronidation by wild-type UGT2B7 (Chau et al. 2014 and unpublished data; Lewis et al. 2007; Stone et al. 2003; Uchaipichat et al. 2006). The Ala and Leu substitutions abolished the glucuronidation of all three substrates. By contrast, morphine 3-glucosidation was unaffected by the Arg259 to Leu substitution, although the Arg259Ala mutant lacked morphine 3-glucosidation activity. The absence of an

Downloaded from molpharm.aspetjournals.org at ASPET Journals on April 19, 2024

Molecular Pharmacology Fast Forward. Published on October 2, 2020 as DOI: 10.1124/molpharm.120.000104
This article has not been copyedited and formatted. The final version may differ from this version.

effect of the Arg259Leu substitution on morphine 3-glucuosidation accords well with the MD simulations that showed Arg259 did not contribute to UDP-Glc binding.

MD simulations of the Arg259Leu mutant with bound UDP-GlcUA showed an altered binding conformation that impacted its interactions with both NT and CT residues (Supplementary Figure S4). For example, the uracil moiety of UDP-GlcUA bound close to Tyr33 in the wild-type UGT2B7 structure, whereas glucuronic acid bound close to this residue in the Arg259Leu mutant. Further, the interactions of UDP-GlcUA with His374, Gln399, Asn398 observed in UGT2B7 were absent in the Arg259Leu mutant. Although the Arg259Leu mutant catalysed morphine 3-glucosidation, MD simulations of Arg259Leu with bound UDP-Glc showed no direct contact between Leu259 and the cofactor, suggesting that bulkiness at this position is essential for maintaining the integrity of the cofactor binding site. This conclusion is in agreement with the observation that UGT3A1 catalyses the glucosidation, but not glucuronidation, of a number of chemicals (Meech et al, 2012). UGT3A1 has Asn, which has a similar volume to Arg, at position 259 (UGT2B7 numbering) (Supplementary Figure S1). By contrast, MD simulations of the Arg259Ala mutant bound with either UDP-GlcUA or UDP-Glc showed conformational changes of residues leading to the loss of nearly all interactions between key binding residues (e.g. Tyr33, Met37, Trp356, Glu382) and UDP-GlcUA, resulting in disorganisation of the cofactor binding domain, suggestive of an unstable protein. The latter observation is consistent with the low expression of the Arg259Ala mutant determined from western blots.

Discussion

UGT2B7 contributes to the elimination of numerous drugs, non-drug xenobiotics and endogenous compounds. The major metabolic pathway catalysed by UGT2B7 is glucuronidation, which utilises UDP-GlcUA as the cofactor. However, as noted previously,

Downloaded from molpharm.aspetjournals.org at ASPET Journals on April 19, 2024

Molecular Pharmacology Fast Forward. Published on October 2, 2020 as DOI: 10.1124/molpharm.120.000104
This article has not been copyedited and formatted. The final version may differ from this version.

this enzyme additionally catalyses the glucosidation of several substrates, including morphine (Chau et al, 2014 and references therein). Our previous analysis of a UGT2B7 homology model suggested that, in addition to the CT domain, residues of the NT domain also contribute to UDP-sugar binding and hence potentially to sugar selectivity. On the basis of our analysis of the homology model (Nair et al. 2015) and on sequence conservation data (Radominska-Pandya et al. 2010), it was postulated that Arg259 may be involved in the selective recognition of UDP-GlcUA. Thus, MD simulations together with SDM and enzyme kinetic studies were performed with wild-type UGT2B7 and the Arg259Ala and Arg259Leu mutants in the absence and presence of bound cofactor (UDP-GlcUA/UDP-Glc) to characterise the relative contributions of the CT and NT domains to cofactor binding and selectivity.

Experimental techniques such as SDM and X-ray crystallography have been utilised previously to gain insights into the structure-function relationships of UGT enzymes. However, these approaches have only provided limited understanding of the contributions of molecular flexibility and dynamic motions of individual residues to cofactor binding and selectivity. By contrast, MD simulations, in combination with experimental approaches, has provided increased knowledge of protein structure-function relationships for several biological systems, including drug metabolising cytochrome P450 enzymes (Nair et al, 2016). Importantly, MD simulations provides a means to model the plasticity of proteins at an atomic level (Nair et al. 2014, 2016). Only two MD simulation studies that investigated ligand binding to UGT proteins (viz. UGT1A6 and UGT1A9/10) have been reported to date (Tripathi et al. 2015; Smith et al. 2020). Neither of these studies provided experimental verification of residues predicted to be involved in UDP-sugar binding, nor insights into the residues that are essential for cofactor selectivity. Further, both studies employed short

Downloaded from molpharm.aspetjournals.org at ASPET Journals on April 19, 2024

Molecular Pharmacology Fast Forward. Published on October 2, 2020 as DOI: 10.1124/molpharm.120.000104
This article has not been copyedited and formatted. The final version may differ from this version.

simulations times (50 ns), which may not be adequate for detailed sampling of conformational space and accurate prediction of protein-ligand interactions. Here, we used long simulation times to generate hypotheses of UDP-sugar selectivity that were tested using SDM and kinetic studies.

Data from MDS highlighted the presence of a handful of residues in the NT domain that contribute to UDP-sugar binding and selectivity. As noted above, Tyr33 was found to be important and formed aromatic pi-pi interaction between Tyr33 and the uracil ring of the UDP-sugar. A previous SDM study from this laboratory demonstrated that the Tyr33Leu mutant lacked glucosidation and glucuronidation activity, whereas the Tyr33Phe mutant retained glycosidation activity (Chau et al., 2014). This is consistent with the importance of aromaticity contributed by Tyr33 for UDP-sugar binding.

Further, MDS demonstrated that the side-chain of Arg259 forms a stable salt-bridge interaction with the carboxylate O group of UDP-GlcUA. Salt-bridges, which occur between oppositely charged groups, are the strongest noncovalent interactions, and are known to contribute significantly to ligand binding (e.g.: Miyamoto et al. 2011; Wester et al., 2004). For instance, the positively charged Arg108 in the active site of CYP2C9 is a key residue in the recognition of the negatively charged weak acids (e.g. carboxylic acids) that are metabolised by this enzyme (Wester et al., 2004). The occurrence of both H-bonding and salt-bridge formation between the UDP-GlcUA and Arg259, which is absent with UDP-Glc, would appear to be the critical factor responsible for the higher binding affinity of UDP-GlcUA to UGT2B7, and is also consistent with glucuronidation being the dominant metabolic pathway for substrates of this enzyme. Moreover, the contribution of NT residues

Downloaded from molpharm.aspetjournals.org at ASPET Journals on April 19, 2024

Molecular Pharmacology Fast Forward. Published on October 2, 2020 as DOI: 10.1124/molpharm.120.000104
This article has not been copyedited and formatted. The final version may differ from this version.

to UDP-GlcUA binding provides a plausible explanation why cofactor does not co-crystallise with the CT domain alone (Miley et al., 2007).

Sequence analysis of human UGT enzymes shows that Arg259 is a conserved residue in UGT 1 and 2 family proteins (Supplementary Figure S1). Consistent with this observation, all members of the UGT 1 and 2 families utilise UDP-GlcUA as a cofactor and hence form glucuronide conjugates. The recent UGT1A6 model reported by Smith et al. (2020) showed the presence of Arg256 (equivalent to Arg259 in UGT2B7) in the cofactor binding site (Supplementary Figure S1). However, this residue interacted with the phosphate group of UDP-GlcUA. Notably, the simulations by Smith et al. (2020) were performed for 50ns and did not reach equilibrium, as the rmsd increased with time. In contrast, our simulations show that the rmsd of the C_α atoms of UGT2B7 in the presence of UDP-Glc (~2.2 Å) and UDP-GlcUA (~2 Å) stabilised after approximately 50 and 100ns, respectively (Supplementary Figure S2), suggesting longer simulation times are essential for attaining equilibrium. Since the stability in the binding interactions involving Arg only occurred after 100ns (Figure 3B and C), crucial side-chain conformations may not be evident with shorter simulations.

In contrast to UGT1 and UGT2 family enzymes, Arg259 (UGT2B7 numbering) is not conserved in UGT 3 and 8 proteins, where the equivalent position is substituted with Asn and Cys, respectively. UGT 3A1, 3A2 and 8 do not utilise UDP-GlcUA (Meech et al., 2012; Meech et al., 2015), further supporting the critical role of the conserved Arg at position 259 (UGT2B7 numbering) in UDP-GlcUA binding.

Miley et al. (2007) solved the first X-ray crystal structure of a human UGT2B7, namely the CT domain of UGT2B7. However, co-crystallisation of the cofactor UDP-GlcUA within the

Downloaded from molpharm.aspetjournals.org at ASPET Journals on April 19, 2024

Molecular Pharmacology Fast Forward. Published on October 2, 2020 as DOI: 10.1124/molpharm.120.000104
This article has not been copyedited and formatted. The final version may differ from this version.

partial UGT2B7 structure was not achieved. Hence, a plant X-ray structure with a bound cofactor (UDP-2-deoxy-2-fluro glucose) was used to predict the binding of UDP-GlcUA within the UGT2B7 protein. The model predicted: a ring-stacking interaction between the conserved Trp356 and uracil, as observed in the plant UGT structure; packing of Gln359 adjacent to the uracil ring; H-bonding of Glu382 to the ribose 2'-OH group; formation of a salt bridge between His374 and the negative charge of the β-phosphate; H-bonding between Asn378 and the α-phosphate; H-bonding of the Thr373 side-chain with the di-phosphate group; and H-bonding of Asp398 and Gln399 with the O3'/O4' and O2'/O3' atoms of glucuronic acid, respectively. Based on these observations and the results of SDM experiments, Miley et al. concluded that disruption of the interactions with either the di-phosphate or glucuronic acid moieties of UGT2B7 abolished activity, whereas disruption of interactions with uracil reduced activity to a moderate extent. Chau et al. (2014) developed a homology model of UGT2B7 based on multiple template structures (UDP-glucose flavonoid 3-*O*-glucosyltransferase, barrel medic UDP-glucose flavonoid/triterpene glucosyltransferase UGT71G1, and the cofactor binding domain of UGT2B7) and employed automated docking to investigate UDP-sugar selectivity. The model predicted identical binding modes for the UDP moiety of UDP-Glc and UDP-GlcUA, but differences in the residues involved in the binding of the sugar moieties. In particular, Asp398 and Glu399 interacted with hydroxyl groups of the glucose, whereas Asn402 and Tyr33 H-bonded with the glucuronic acid moiety of UDP-GlcUA.

There are no X-ray crystal structures of a UDP-GlcUA bound mammalian UGT protein, and the currently available models are based on the assumption that UDP-Glc and UDP-GlcUA interact identically with residues in the cofactor binding site (Miley et al., 2007). Notably, the existing models that predict the UGT-UDP-GlcUA interactions are based on the analysis of

Downloaded from molpharm.aspetjournals.org at ASPET Journals on April 19, 2024

Molecular Pharmacology Fast Forward. Published on October 2, 2020 as DOI: 10.1124/molpharm.120.000104
This article has not been copyedited and formatted. The final version may differ from this version.

plant UGT X-ray structures, where the cofactor is either UDP-Glc or UDP-Glc analogues. Furthermore, UGT2B7 models based on docking UDP-GlcUA in the static protein do not provide a clear basis for UDP-sugar binding or selectivity (Chau et al., 2014). Overall, our simulations demonstrate that the binding interactions of UDP-Glc and UDP-GlcUA at the CT domain, although not identical, are very similar with only subtle variations involving the adaptive repositioning of residues within the binding site for cofactor recognition.

Previous studies that utilised static models predicted Tyr33, Asn378 and Asn402 of UGT2B7 were important for UDP-sugar selectivity, and as noted above mutagenesis of these amino acids led to loss of all glycosidation activity (Miley et al., 2007; Chau et al., 2014). As described above, simulations demonstrated that Tyr33 is located close to the uracil ring of the UDP-sugar, whereas Asn402 interacts with the –OH group of the sugar rings with no direct interaction with the $–CO_2^-$ or $–CH_2OH$ groups of UDP-GlcUA or UDP-Glc, respectively. This suggests that both residues may be important for UDP-sugar binding, but not sugar selectivity. Further, as noted in the simulations with bound UDP-GlcUA, Arg259 H-bonds with Asn378 allowing the Arg side-chain to form a stable salt-bridge with the carboxylate group of UDP-GlcUA. The SDM results reported here demonstrated that the Arg259Leu mutant catalysed the glucosidation but not glucuronidation of morphine, indicating that Arg259 (and not Asn378) is the critical residue for the selective binding of UDP-GlcUA over UDP-Glc.

Conclusions

This is the first structure-function study of a UGT enzyme that has employed MD simulations for hypothesis generation, with subsequent experimental verification. The study demonstrated the importance of structural flexibility and the physicochemical properties of amino acids in the selective binding of UDP-sugars within UGT2B7 active site. In particular, Arg259,

Downloaded from molpharm.aspetjournals.org at ASPET Journals on April 19, 2024

Molecular Pharmacology Fast Forward. Published on October 2, 2020 as DOI: 10.1124/molpharm.120.000104
This article has not been copyedited and formatted. The final version may differ from this version.

located in the NT, was shown to be critical for binding the carboxylate group of glucuronic acid via H-bonding and salt-bridge formation. The study further demonstrated that conformational equilibrium and stable interactions between UDP-GlcUA and cofactor binding site residues was only achieved with simulation times > 100 ns, suggesting that shorter simulations may present incomplete sampling and crucial conformational rearrangements may be overlooked.

Downloaded from molpharm.aspetjournals.org at ASPET Journals on April 19, 2024

Molecular Pharmacology Fast Forward. Published on October 2, 2020 as DOI: 10.1124/molpharm.120.000104
This article has not been copyedited and formatted. The final version may differ from this version.

MOLPHARM-AR-2020-000104

Acknowledgements

This study was supported by a project grant [1120137] from the National Health and Medical Research Council of Australia. This research was undertaken with the assistance of resources from the National Computational Infrastructure (NCI), which is supported by the Australian Government. PCN acknowledges Flinders University for Early Career Research Funding. RAM is a Beat Cancer Professorial Fellow supported by Cancer Council SA and SA Health.

Downloaded from molpharm.aspetjournals.org at ASPET Journals on April 19, 2024

Molecular Pharmacology Fast Forward. Published on October 2, 2020 as DOI: 10.1124/molpharm.120.000104
This article has not been copyedited and formatted. The final version may differ from this version.

MOLPHARM-AR-2020-000104

AUTHORSHIP CONTRBUTIONS

Participated in research design: Nair, Miners, Chau, McKinnon.

Conducted experiments: Nair, Chau.

Contributed new reagents or analytic tools: Nair, Miners, McKinnon.

Performed data analysis: Nair, Chau, Miners, McKinnon.

Wrote or contributed to the writing of the manuscript: Nair, Miners, Chau, McKinnon.

Downloaded from molpharm.aspetjournals.org at ASPET Journals on April 19, 2024

Molecular Pharmacology Fast Forward. Published on October 2, 2020 as DOI: 10.1124/molpharm.120.000104
This article has not been copyedited and formatted. The final version may differ from this version.

References

References

Abraham MJ, Murtola T, Schulz R, Páll S, Smith JC, Hess B, and Lindahl E (2015). GROMACS: High performance molecular simulations through multi-level parallelism from laptops to supercomputers. SoftwareX **1–2:**19–25.

Chau N, Elliot D J, Lewis BC, Burns K, Johnston MR, Mackenzie PI, et al. (2014). Morphine glucuronidation and glucosidation represent complementary metabolic pathways that are both catalyzed by UDP-glucuronosyltransferase 2B7: kinetic, inhibition, and molecular modeling studies. J Pharmacol Exp Ther **349:**126-37.

Court MH, Krishnaswamy S, Hao Q, Duan SX, Patten CJ, Von Moltke LL, Greenblatt DJ (2003). Evaluation of 3'-azido-3'-deoxythymidine, morphine, and codeine as probe substrates for UDP-glucuronosyltransferase 2B7 (UGT2B7) in human liver microsomes: specificity and influence of the UGT2B7*2 polymorphism. Drug Metab Dispos **31:**1125-33.

Darden T, York D, Pedersen L (1993). Particle mesh Ewald: An N·log(N) method for Ewald sums in large systems. J Chem Phys **98:**10089.

Essmann U, Perera L, Berkowitz ML, Darden T, Lee H, Pedersen LG (1995). A smooth particle mesh Ewald method. J Chem Phys **103:**8577-8593.

Feingold DS, Franzen JS. (1981). Pyridine nucleotide-linked four-electron transfer dehydrogenases. Trends in Biochemical Sciences **6:**103-105

Downloaded from molpharm.aspetjournals.org at ASPET Journals on April 19, 2024

Molecular Pharmacology Fast Forward. Published on October 2, 2020 as DOI: 10.1124/molpharm.120.000104
This article has not been copyedited and formatted. The final version may differ from this version.

Hoover WG (1985). Canonical dynamics: Equilibrium phase-space distributions. Phys Rev A, Gen Phys **31:**1695–1697.

Kerdpin, O., Mackenzie, P. I., Bowalgaha, K., Finel, M., Miners, J. O. (2009). Influence of N-terminal domain histidine and proline residues on the substrate selectivities of human UDP-glucuronosyltransferase 1A1, 1A6, 1A9, 2B7, and 2B10. Drug Metab Dispos **37:**1948-55.

Lewis, BC, Mackenzie, PI, Elliot, DJ, Burchell, B, Bhasker, CR & Miners, JO (2007). Amino terminal domains of human UDP-glucuronosyltransferases (UGT) 2B7 and 2B15 associated with substrate selectivity and autoactivation, Biochemical Pharmacology, **73:**1463-1473.

Mackenzie PI, Rogers A, Treloar J, Jorgensen BR, Miners JO, Meech R (2008). Identification of UDP glycosyltransferase 3A1 as a UDP N-acetylglucosaminyltransferase Journal of Biological Chemistry **283:**36205-36210.

Mackenzie PI, Bock KW, Burchell B, Guillemette C, Ikushiro S, Iyanagi T, Miners JO, Owens IS, and Nebert DW (2005). Nomenclature update for the mammalian UDP glycosyltransferase (UGT) gene superfamily. Pharmacogenet Genomics **15:** 677–685.

Mackenzie, PI, Owens, I. S., Burchell, B., Bock, K. W., Bairoch, A., Belanger, A., et al. (1997). The UDP glycosyltransferase gene superfamily: recommended nomenclature update based on evolutionary divergence. Pharmacogenetics **7:**255-269.

Downloaded from molpharm.aspetjournals.org at ASPET Journals on April 19, 2024

Molecular Pharmacology Fast Forward. Published on October 2, 2020 as DOI: 10.1124/molpharm.120.000104
This article has not been copyedited and formatted. The final version may differ from this version.

Malde AK, Zuo L, Breeze M, Stroet M, Poger D, Nair PC, Oostenbrink C, and Mark AE (2011). An Automated Force Field Topology Builder (ATB) and Repository: Version 1.0. J Chem Theory Comput **7:**4026–4037.

Meech R, Rogers A, Zhuang L, Lewis BC, Miners JO, Mackenzie PI. (2012). Identification of residues that confer sugar selectivity to UDP-glycosyltransferase 3A (UGT3A) enzymes. J Biol Chem. **287:**24122-30.

Meech R, Hu DG, McKinnon RA, Mubarokah SN, Haines AZ, Nair PC, Rowland A, Mackenzie PI. (2019). The UDP-Glycosyltransferase (UGT) Superfamily: New Members, New Functions, and Novel Paradigms. Physiol Rev. **99:**1153-1222.

Meech, R., Mubarokah, N., Shivasami, A., Rogers, A., Nair, P. C., Hu, D. G., et al. (2015). A novel function for UDP glycosyltransferase 8: galactosidation of bile acids. Mol Pharmacol **87:**442-50.

Miley MJ, Zielinska AK, Keenan JE, et al. (2007). Crystal structure of the cofactor-binding domain of the human phase II drug-metabolism enzyme UDP-glucuronosyltransferase 2B7. J Mol Biol **369:**498–511.

Miners JO, Mackenzie PI (1991). Drug glucuronidation in humans. Pharmacology & Therapeutics **51:**347-369.

Downloaded from molpharm.aspetjournals.org at ASPET Journals on April 19, 2024

Molecular Pharmacology Fast Forward. Published on October 2, 2020 as DOI: 10.1124/molpharm.120.000104
This article has not been copyedited and formatted. The final version may differ from this version.

Miners JO, Smith PA, Sorich MJ, McKinnon RA, Mackenzie PI (2004). Predicting Human Drug Glucuronidation Parameters: Application of In Vitro and In Silico Modeling Approaches. Annu Rev Pharmacol Toxicol **44:**1-25.

Miners JO, Mackenzie PI and Knights KM (2010). The prediction of drug-glucuronidation parameters in humans: UDP-glucuronosyltransferase enzyme-selective substrate and inhibitor probes for reaction phenotyping and in vitro-in vivo extrapolation of drug clearance and drug-drug interaction potential. Drug Metabolism Reviews **42:**196-208.

Miyamoto Y, Banno Y, Yamashita T, Fujimoto T, Oi S, Moritoh Y, Asakawa T, Kataoka O, Yashiro H, Takeuchi K, Suzuki N, Ikedo K, Kosaka T, Tsubotani S, Tani A, Sasaki M, Funami M, Amano M, Yamamoto Y, Aertgeerts K, Yano J, Maezaki H. (2011). Discovery of a 3-pyridylacetic acid derivative (TAK-100) as a potent, selective and orally active dipeptidyl peptidase IV (DPP-4) inhibitor. J Med Chem **54:**831-50.

Nair PC, Meech R, Mackenzie PI, McKinnon RA, Miners JO (2015). Insights into the UDP-sugar selectivities of human UDP-glycosyltransferases (UGT): a molecular modeling perspective. Drug Metab Rev **47:**335-45.

Nair PC, Miners JO (2014). Molecular dynamics simulations: from structure function relationships to drug discovery. In Silico Pharmacology **2:**4.

Nair PC, McKinnon RA, Miners JO (2016). Cytochrome P450 structure–function: insights from molecular dynamics simulations. Drug Metabolism Reviews **48:** 434-452.

Downloaded from molpharm.aspetjournals.org at ASPET Journals on April 19, 2024

Molecular Pharmacology Fast Forward. Published on October 2, 2020 as DOI: 10.1124/molpharm.120.000104
This article has not been copyedited and formatted. The final version may differ from this version.

Nosé S. (1984). A unified formulation of the constant temperature molecular dynamics methods. J Chem Phys **81:**511.

Offen W, Martinez-Fleites C, Yang M, Kiat-Lim E, Davis BG, Tarling CA, Ford CM, Bowles DJ, Davies GJ. (2006). Structure of a flavonoid glucosyltransferase reveals the basis for plant natural product modification. EMBO J **25:**1396-405.

Parrinello M, and Rahman A (1981). Polymorphic transitions in single crystals: A new molecular dynamics method. J Appl Phys **52:**7182–7190.

Radominska-Pandya A, Czernik PJ, Little JM, Battaglia E, and Mackenzie PI (1999). Structural and functional studies of UDP-glucuronosyltransferases. Drug Metab Rev **31:**817–899.

Radominska-Pandya A, Little JM, Czernik PJ (2001). Human UDP-glucuronosyltransferase 2B7. Current Drug Metabolism **2:**283.

Radominska-Pandya, A., Bratton, S. M., Redinbo, M. R., Miley, M. J. (2010). The crystal structure of human UDP-glucuronosyltransferase 2B7 C-terminal end is the first mammalian UGT target to be revealed: the significance for human UGTs from both the 1A and 2B families. Drug Metab Rev **42:**133-44.

Rowland, A, Gaganis, P, Elliot, DJ, Mackenzie, PI, Knights, KM & Miners, JO (2007). Binding of inhibitory fatty acids is responsible for the enhancement of UDP-

Downloaded from molpharm.aspetjournals.org at ASPET Journals on April 19, 2024

Molecular Pharmacology Fast Forward. Published on October 2, 2020 as DOI: 10.1124/molpharm.120.000104
This article has not been copyedited and formatted. The final version may differ from this version.

glucuronosyltransferase 2B7 activity by albumin: implications for in vitro-in vivo extrapolation, J Pharmacol Exp Ther **321:**137-147.

Smith AD, Page BDG, Collier AC, Coughtrie MWH (2020). Homology Modeling of Human Uridine-5'-diphosphate-glucuronosyltransferase 1A6 Reveals Insights Into Factors Influencing Substrate and Cosubstrate Binding. ACS Omega **5:**6872-6887

Stingl JC, Bartels H, Viviana R, Lehmann ML, Brockemoller J. (2014). Relevance of UDP-glucuronosyltransferase polymorphisms for drug dosing: quantitative systematic review. Pharmacol Ther **141:**92-116.

Stone AN, Mackenzie PI, Galetin A, Houston JB, Miners JO. (2003). Isoform selectivity and kinetics of morphine 3- and 6-glucuronidation by human udp-glucuronosyltransferases: evidence for atypical glucuronidation kinetics by UGT2B7. Drug Metab Dispos **31:**1086-9.

The PyMOL Molecular Graphics System, Version 2.0 Schrödinger, LLC.

Tripathi SP, Prajapati R, Verma N, Sangamwar AT (2016). Predicting substrate selectivity between UGT1A9 and UGT1A10 using molecular modelling and molecular dynamics approach, Molecular Simulation **42:**270-288.

Uchaipichat V, Galetin A, Houston JB, Mackenzie PI, Williams JA, and Miners JO (2008). Kinetic modeling of the interactions between 4-methylumbelliferone, 1-naphthol, and zidovudine glucuronidation by UDP-glucuronosyltransferase 2B7 (UGT2B7) provides evidence for multiple substrate binding and effector sites. Mol Pharmacol **74:**1152–1162.

Downloaded from molpharm.aspetjournals.org at ASPET Journals on April 19, 2024

Molecular Pharmacology Fast Forward. Published on October 2, 2020 as DOI: 10.1124/molpharm.120.000104
This article has not been copyedited and formatted. The final version may differ from this version.

Uchaipichat V, Mackenzie PI, Guo X-H, Gardner-Stephen D, Galetin A, Houston JB, and Miners JO (2004). Human udp-glucuronosyltransferases: isoform selectivity and kinetics of 4-methylumbelliferone and 1-naphthol glucuronidation, effects of organic solvents, and inhibition by diclofenac and probenecid. Drug Metab Dispos **32:**413–423.

Uchaipichat V, Raungrut P, Chau N, Janchawee B, Evans AM, Miners JO (2011). Effects of ketamine on human UDP-glucuronosyltransferases in vitro predict potential drug-drug interactions arising from ketamine inhibition of codeine and morphine glucuronidation. Drug Metab Dispos **39:**1324-1328.

Uchaipichat, V, Winner, LK, Mackenzie, PI, Elliot, DJ, Williams, JA & Miners, JO (2006). Quantitative prediction of in vivo inhibitory interactions involving glucuronidated drugs from in vitro data: the effect of fluconazole on zidovudine glucuronidation. BJCP 61:427-439.

Valley CC, Cembran A, Perlmutter JD, Lewis AK, Labello NP, Gao J, Sachs JN. (2012). The methionine-aromatic motif plays a unique role in stabilizing protein structure J. Biol. Chem. **287:**34979-34991.

Weber DS and Warren JJ. (2019). The Interaction Between Methionine and Two Aromatic Amino Acids Is an Abundant and Multifunctional Motif in Proteins. Arch Biochem Biophys **672:**108053.

Downloaded from molpharm.aspetjournals.org at ASPET Journals on April 19, 2024

Molecular Pharmacology Fast Forward. Published on October 2, 2020 as DOI: 10.1124/molpharm.120.000104
This article has not been copyedited and formatted. The final version may differ from this version.

Wester MR, Yano JK, Schoch GA, Yang C, Griffin KJ, Stout CD, Johnson EF (2004). The Structure of Human Cytochrome P450 2C9 Complexed with Flurbiprofen at 2.0-A Resolution. J Biol Chem **279:**35630-7.

Zhang L, Zhu L, Qu W, Wu F, Hu M, Xie W, Liu Z, Wang C (2020). Insight into tartrate inhibition patterns in vitro and in vivo based on cocrystal structure with UDP-glucuronosyltransferase 2B15. Biochem Pharmacol. **172:**113753.

Downloaded from molpharm.aspetjournals.org at ASPET Journals on April 19, 2024

Molecular Pharmacology Fast Forward. Published on October 2, 2020 as DOI: 10.1124/molpharm.120.000104
This article has not been copyedited and formatted. The final version may differ from this version.

MOLPHARM-AR-2020-000104

Footnotes

This study was supported by a project grant [1120137] from the National Health and Medical Research Council of Australia.

Downloaded from molpharm.aspetjournals.org at ASPET Journals on April 19, 2024

Molecular Pharmacology Fast Forward. Published on October 2, 2020 as DOI: 10.1124/molpharm.120.000104
This article has not been copyedited and formatted. The final version may differ from this version.

Figure Legends

Figure 1: (A) The homology model of UGT2B7 developed using the X-ray crystal structure of UGT85H2 from *Medicago truncatula*. (B) Enlarged view of the UDP-sugar binding site along with key residues involved in catalysis (sticks). The N- and C-terminal domains are shown in green and yellow, respectively, while the signature sequence is shown in red.

Figure 2: MD simulations of cofactor bound UGT2B7. (A) Binding mode of UDP-Glc, and (B) binding mode of UDP-GlcUA showing the average position of side-chain residues. The CT domain is shown in purple (surface), the signature sequence in yellow (transparent surface), and amino acids important for cofactor binding as yellow sticks (C atoms). The NT domain residues are shown as green sticks (C atoms). O, N, S and P atoms are shown in red, blue, yellow and orange, respectively.

Figure 3: (A) Distance between the side-chain of Arg259 (-NH) and -CH_2OH (O) of UDP-Glc. (B) Distance between the side-chain of Arg259 (-NH) and the -COO^- (O) of UDP-GlcUA. (C) Distance between the N atom of the Arg259 side-chain and the -COO^- (O atoms) of UDP-GlcUA.

Figure 4: 4-MU, AZT and morphine glucuronidation (A-D) and morphine glucosidation (E) activities of wild-type UGT2B7 and the Arg259Ala and Arg259Leu mutants. Activities shown as mean ± standard deviation (SD) (n=4). The absence of bars indicates no measurable activity.

Downloaded from molpharm.aspetjournals.org at ASPET Journals on April 19, 2024

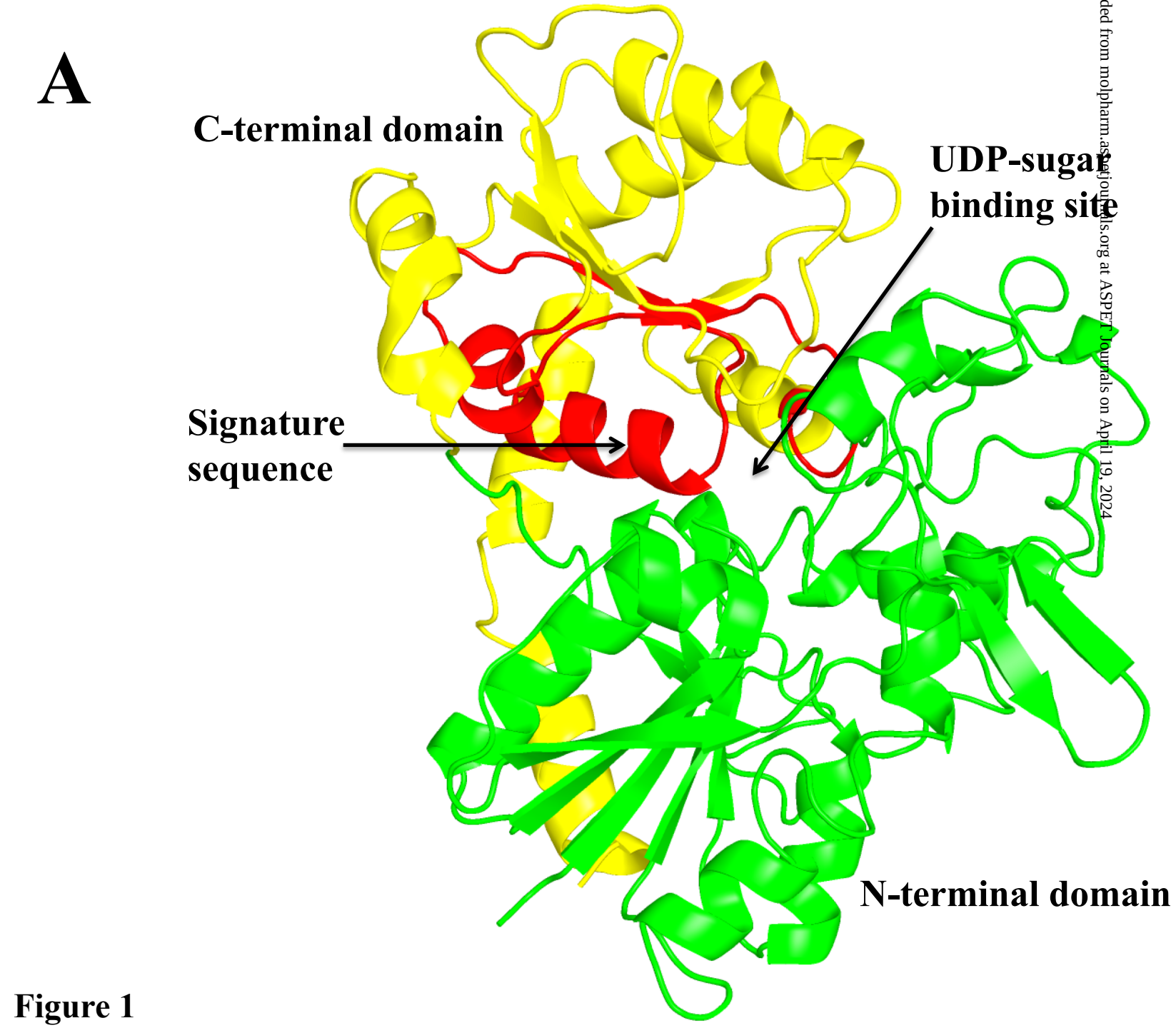

ded from molpharm.aspetjournals.org at ASPET Journals on April 19, 2024

Figure 1

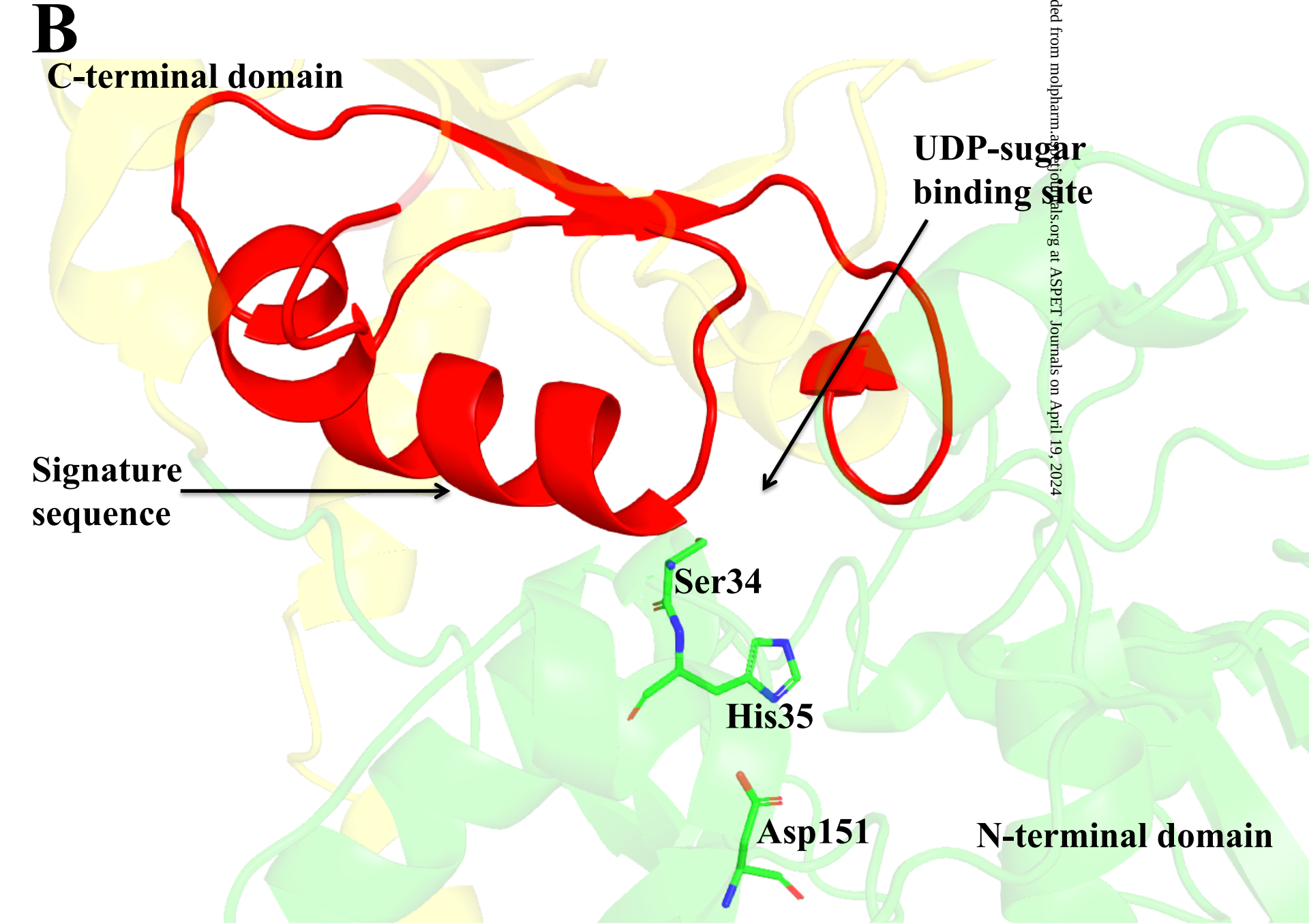

ded from molpharm.aspetjournals.org at ASPET Journals on April 19, 2024

Figure 1

Molecular Pharmacology Fast Forward. Published on October 2, 2020 as DOI: 10.1124/molpharm.120.000104
This article has not been copyedited and formatted. The final version may differ from this version.

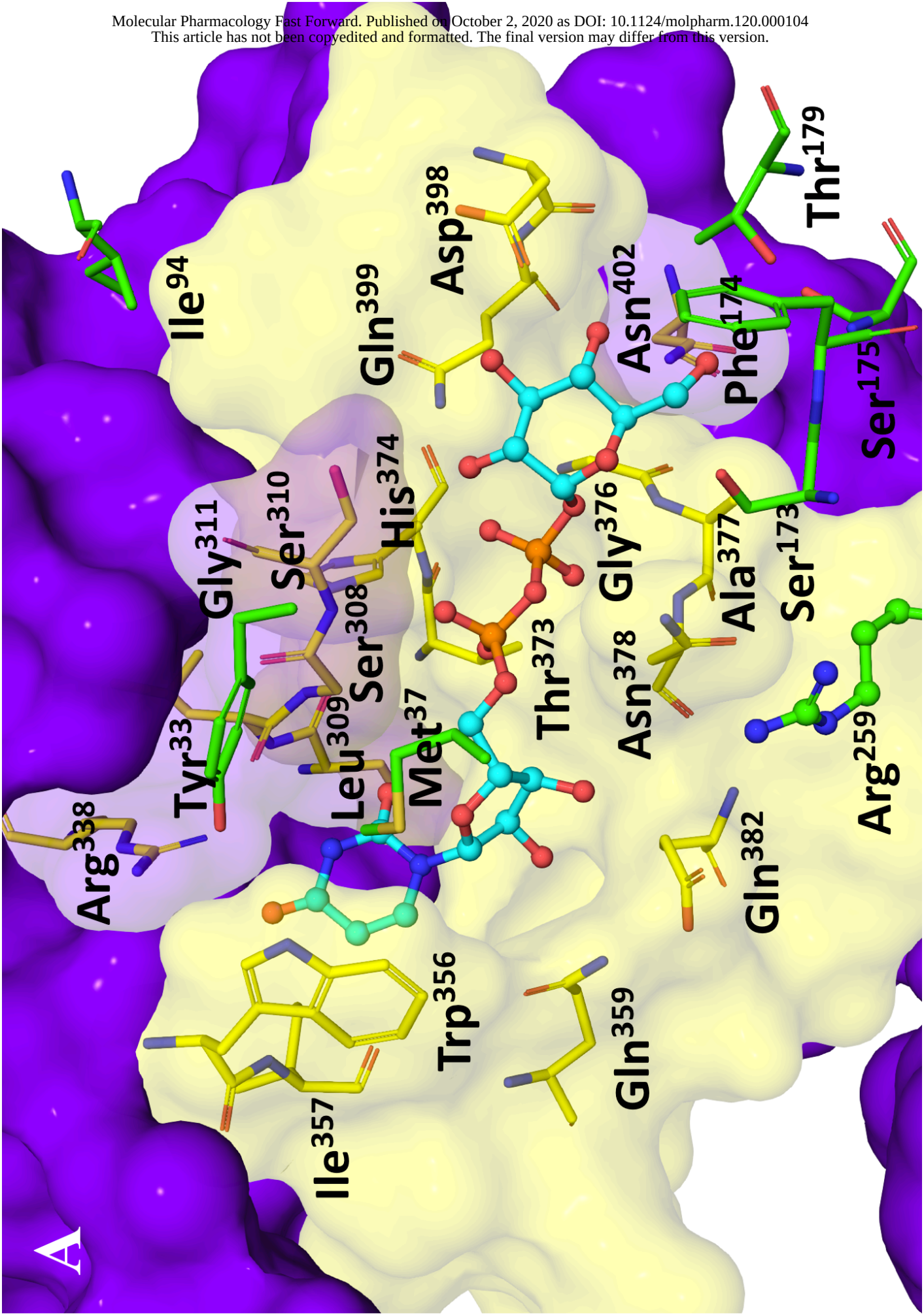

Figure 2

Downloaded from molpharm.aspetjournals.org at ASPET Journals on April 19, 2024

Molecular Pharmacology Fast Forward. Published on October 2, 2020 as DOI: 10.1124/molpharm.120.000104
This article has not been copyedited and formatted. The final version may differ from this version.

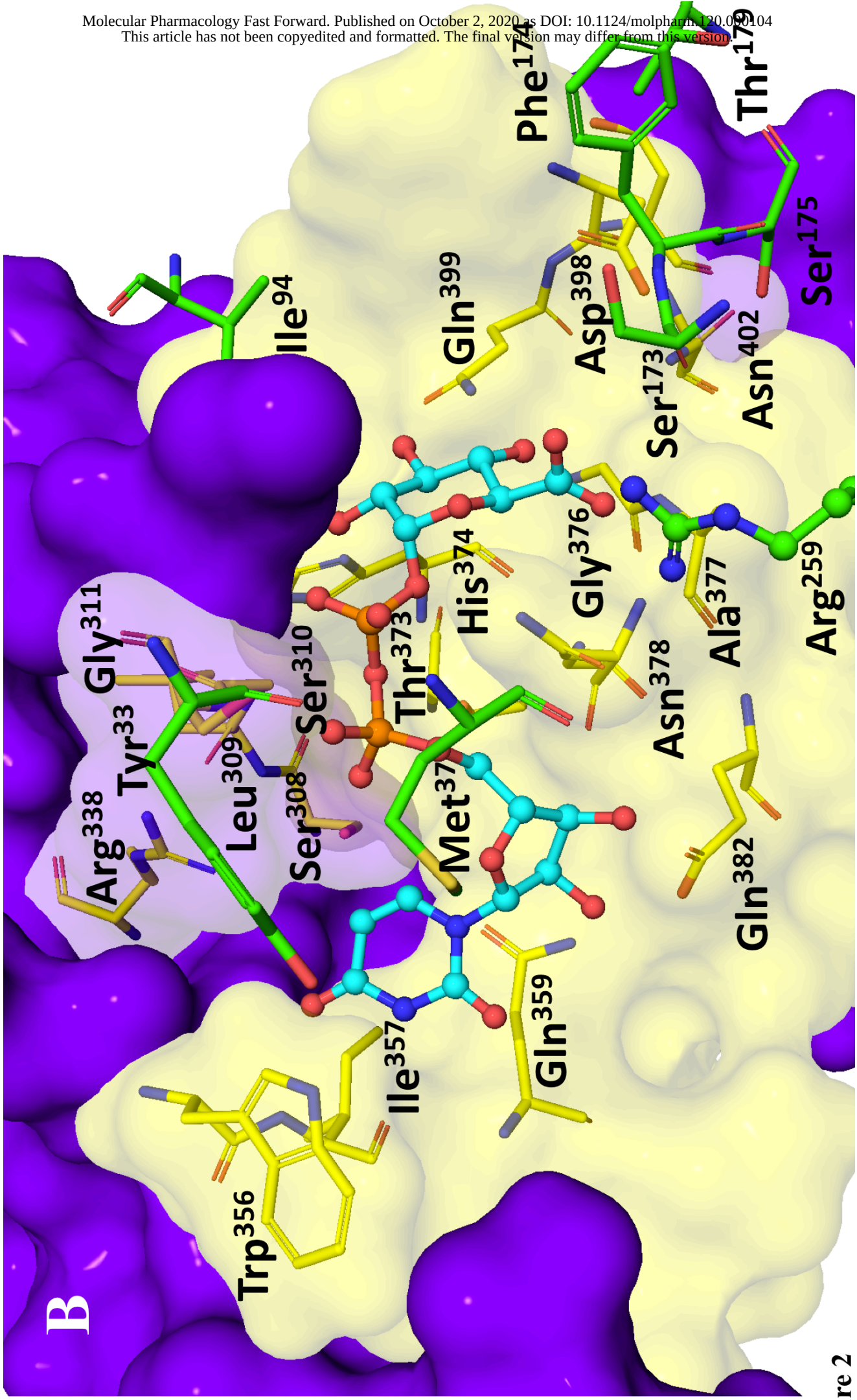

Figure 2

Downloaded from molpharm.aspetjournals.org at ASPET Journals on April 19, 2024

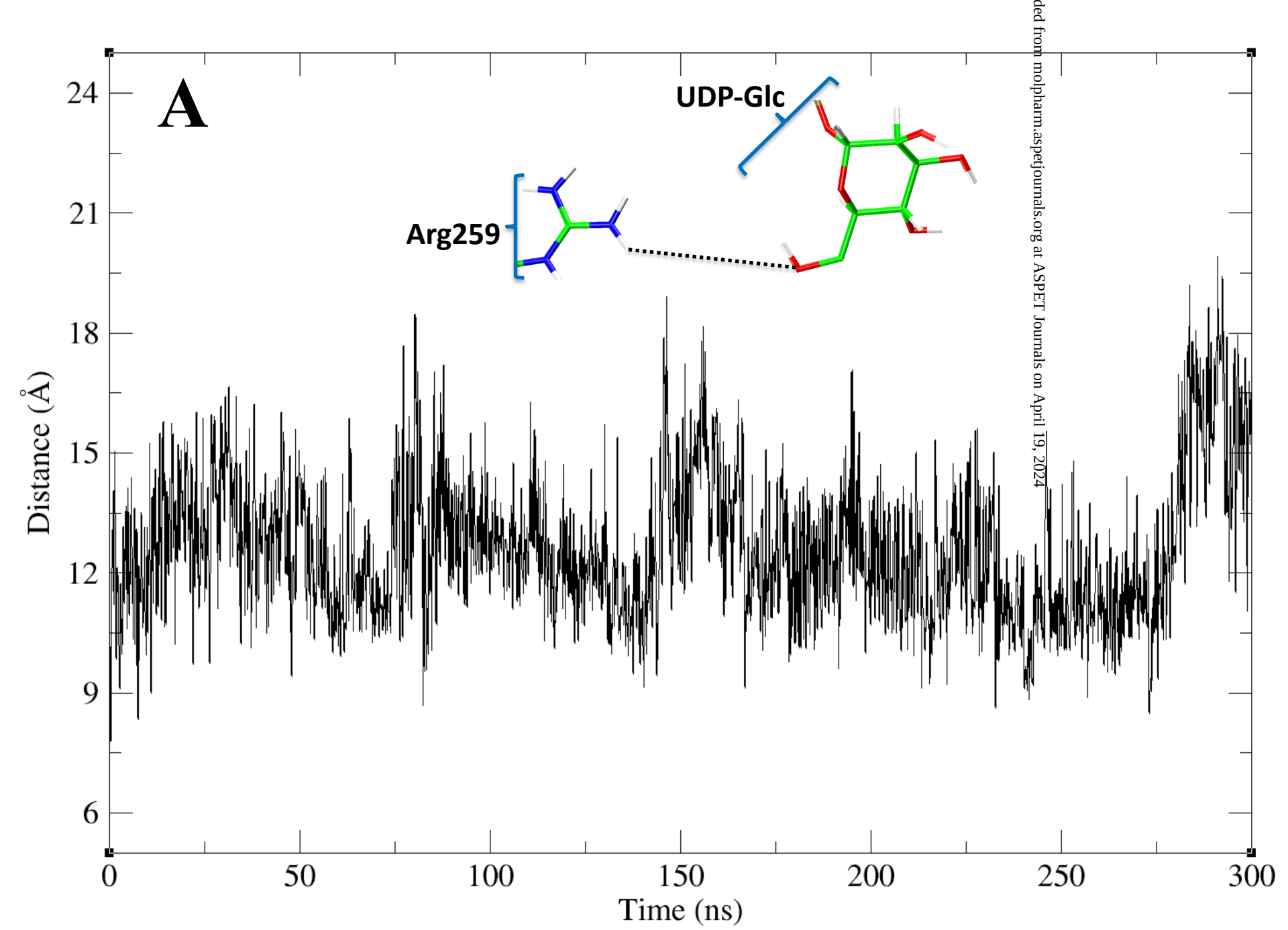

ded from molpharm.aspetjournals.org at ASPET Journals on April 19, 2024

Figure 3

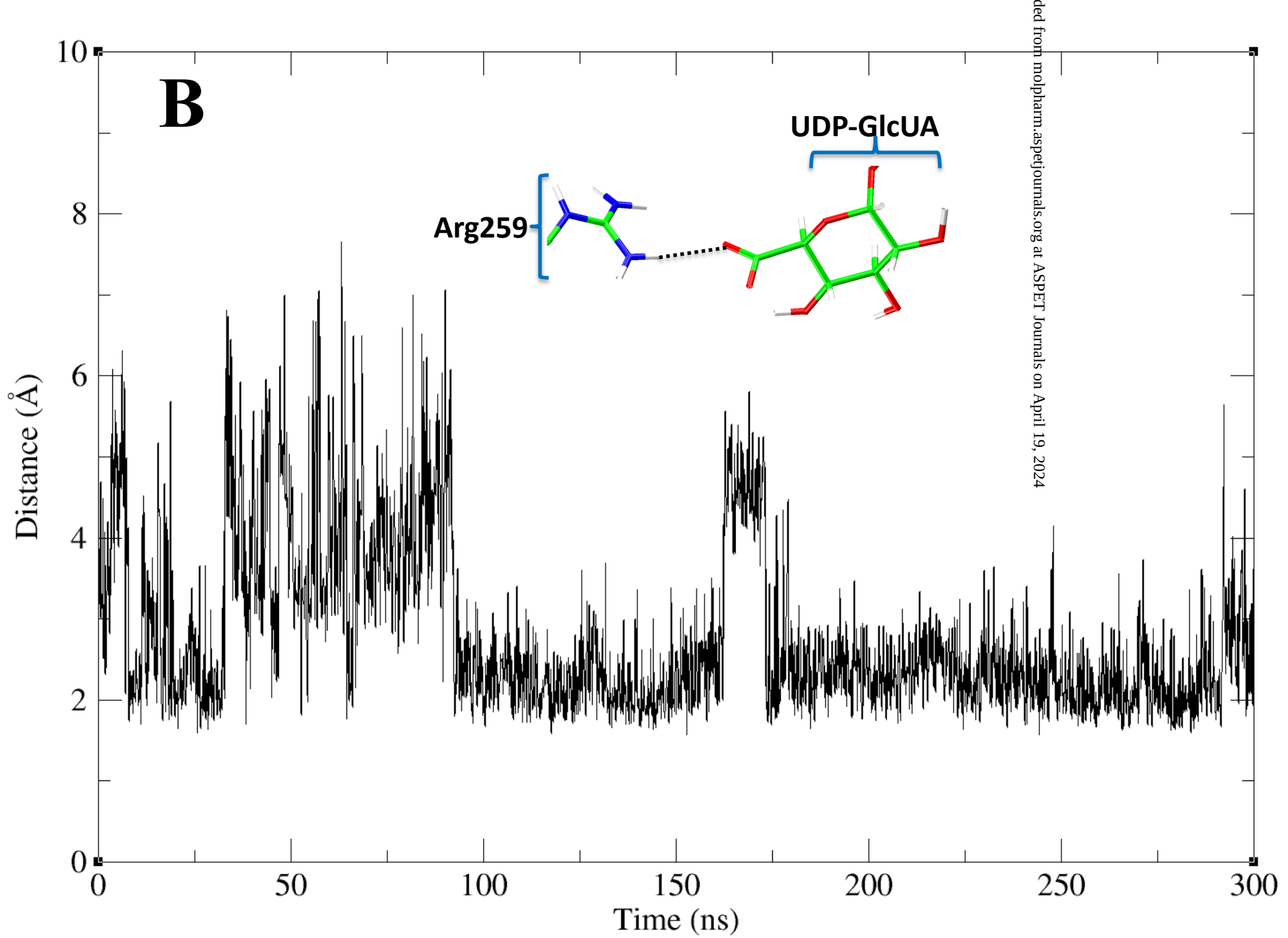

ded from molpharm.aspetjournals.org at ASPET Journals on April 19, 2024

Figure 3

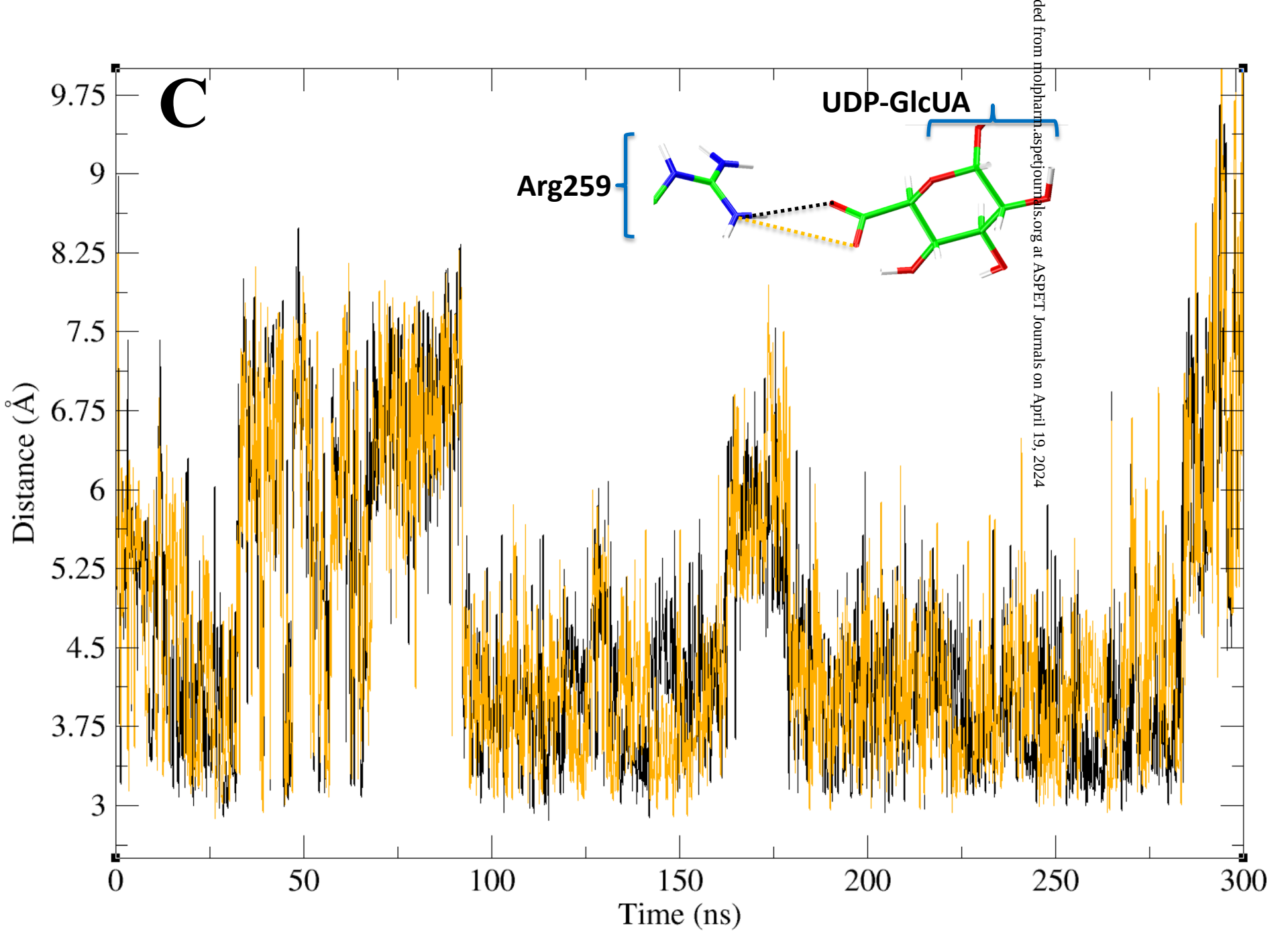

ded from molpharm.aspetjournals.org at ASPET Journals on April 19, 2024

Figure 3

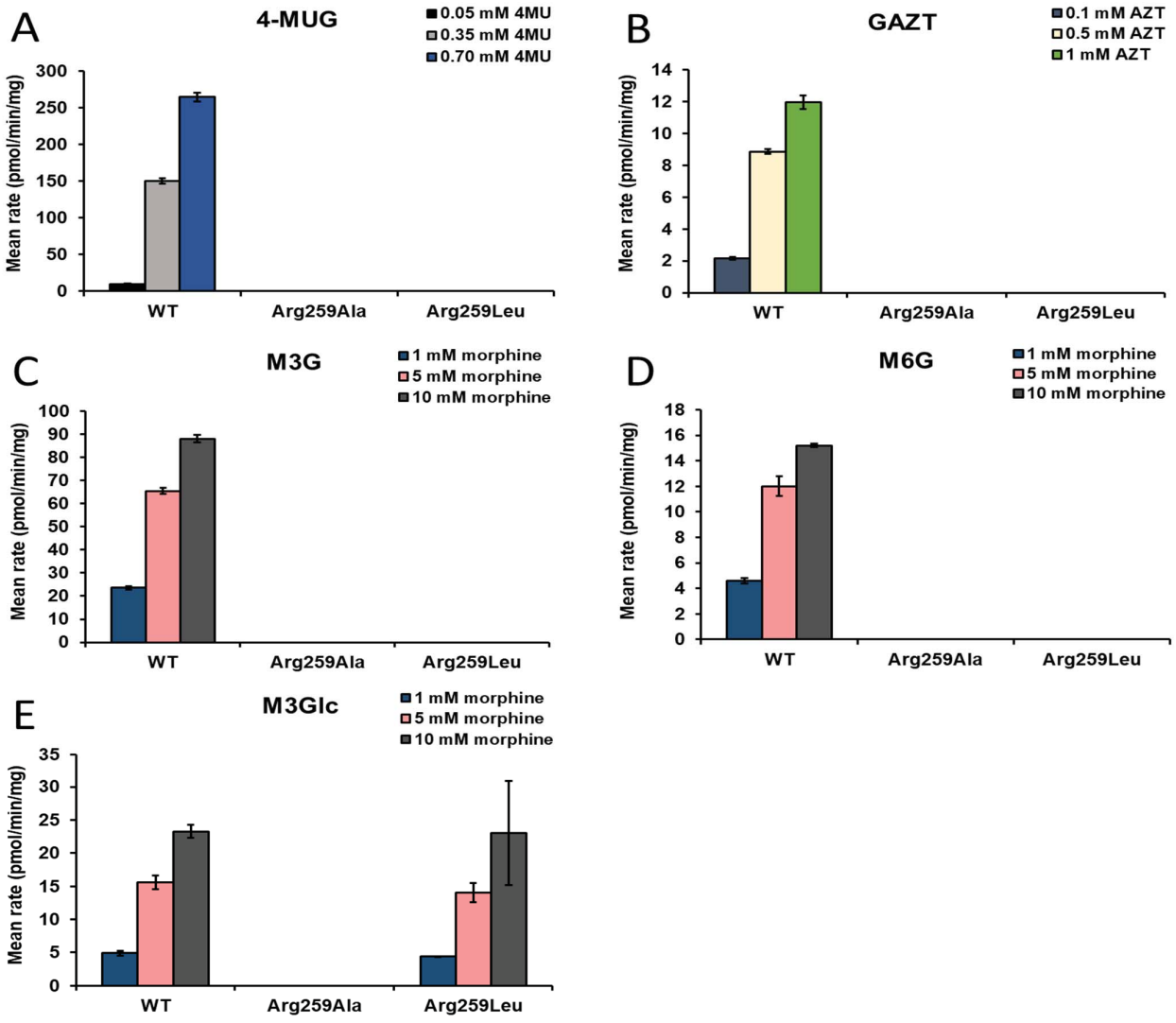

Figure 4

Downloaded from molpharm.aspetjournals.org at ASPET Journals on April 19, 2024

MOLPHARM-AR-2020-000104

Supplemental data

Arginine-259 of UDP-glycosyltransferase 2B7 (UGT2B7) confers UDP-sugar selectivity

Pramod C. Nair[1,2#], Nuy Chau[1#], Ross A. McKinnon[2] and John O. Miners[1,2]

[1]Department of Clinical Pharmacology, Flinders University College of Medicine and Public Health, Flinders Medical Centre, Bedford Park, SA 5042, Australia.

[2] FHMRI Cancer Program, Flinders Health and Medical Research Institute, Flinders University College of Medicine and Public Health, Flinders Medical Centre, Bedford Park, SA 5042, Australia.

#Joint first authors.

Table S1. Oligonucleotide primers used for site-directed mutagenesis. Nucleobase(s) mutated are highlighted in blue.

Mutant	Primer (5′ to 3′)	
	Forward	Reverse
R259A	GCTGACGTATGGCTTATT**GC**AAACTCCTGG	GGAAACTGAAAATTCCAGGAGTTT**GC**AATAAGCC
R259L	GCTGACGTATGGCTTATTC**T**AAACTCCTGG	GGAAACTGAAAATTCCAGGAGTTT**A**GAATAAGCC

```
UGT1A1    227YSPYATLASE-FLQREVTVQDLLSSASVWLFRSDFVKDYPRPIMPNMVFVGGINCLHQNP285
UGT1A3    228SAPYASLASE-LFQREVSVVDILSHASVWLFRGDFVMDYPRPIMPNMVFIGGINCANRKP286
UGT1A4    228SAPYASLASE-LFQREVSVVDLVSYASVWLFRGDFVMDYPRPIMPNMVFIGGINCANGKP286
UGT1A5    228SAPYASLASE-LFQREVSVVDLVSHASVWLFRGDFVMDYPRPIMPNMVFIGGINCANGKP286
UGT1A6    226FSKYEELASA-VLKRDVDIITLYQKVSVWLLRYDFVLEYPRPVMPNMVFIGGINCKKRKD284
UGT1A7    224FKNVLEIASE-ILQTPVTAYDLYSHTSIWLLRTDFVLEYPKPVMPNMIFIGGINCHQGKP282
UGT1A8    224SKNALEIASE-ILQTPVTAYDLYSHTSIWLLRTDFVLDYPKPVMPNMIFIGGINCHQGKP282
UGT1A9    224FKNALEIASE-ILQTPVTEYDLYSHTSIWLLRTDFVLDYPKPVMPNMIFIGGINCHQGKP282
UGT1A10   224FRNALEIASE-ILQTPVTAYDLYSHTSIWLLRTDFVLDYPKPVMPNMIFIGGINCHQGKP282
UGT2A1    227WKSWDSYYSK-ALGRPTTLCETMGKAEIWLIRTYWDFEFPRPYLPNFEFVGGLHCKPAKP285
UGT2A3    227YHFWEEFYSK-ALGRPTTLCETVGKAEIWLIRTYWDFEFPQPYQPNFEFVGGLHCKPAKA285
UGT2B4    229MKKWDQFYSE-VLGRPTTLSETMAKADIWLIRNYWDFQFPHPLLPNVEFVGGLHCKPAKP287
UGT2B7    229MKKWDQFYSE-VLGRPTTLSETMGKADVWLIRNSWNFQFPYPLLPNVDFVGGLHCKPAKP287
UGTB10    228MKKWDQFYSE-VLGRPTTLSETMRKADIWLMRNSWNFKFPHPFLPNVDFVGGLHCKPAKP286
UGTB11    229MKKWDQFYSE-VLGRPTTLFETMGKADIWLMRNSWSFQFPHPFLPNVDFVGGFHCKPAKP287
UGTB15    230LKKWDQFYSE-VLGRPTTLFETMGKAEMWLIRTYWDFEFPRPFLPNVDFVGGLHCKPAKP288
UGTB17    230LKKWDQFYSE-VLGRPTTLFETMGKAEMWLIRTYWDFEFPRPFLPNVDFVGGLHCKPAKP288
UGTB28    229MKKWDQFYSE-VLGRPTTLFETMGKADIWLMRNSWSFQFPHPFLPNIDFVGGLHCKPAKP287
UGT3A1    219STFDNTIKEHFPEGSRPVLSHLLLKAELWFVNSDFAFDFARPLLPNTVYIGGLMEKPIKP278
UGT3A2    219STFDNTIKEHFTEGSRPVLSHLLLKAELWFINSDFAFDFARPLLPNTVYVGGLMEKPIKP278
UGT8A1    212LPKYERIMQKYNLLPEKSMYDLVHGSSLWMLCTDVALEFPRPTLPNVVYVGGILTKPASP271
```

Figure S1 Sequence alignment of residues 229-287 (UGT2B7 numbering) of UGT family 1,2 and 3 enzymes. Arg259 (UGT2B7 numbering) and the equivalent position in all UGTs are highlighted in blue.

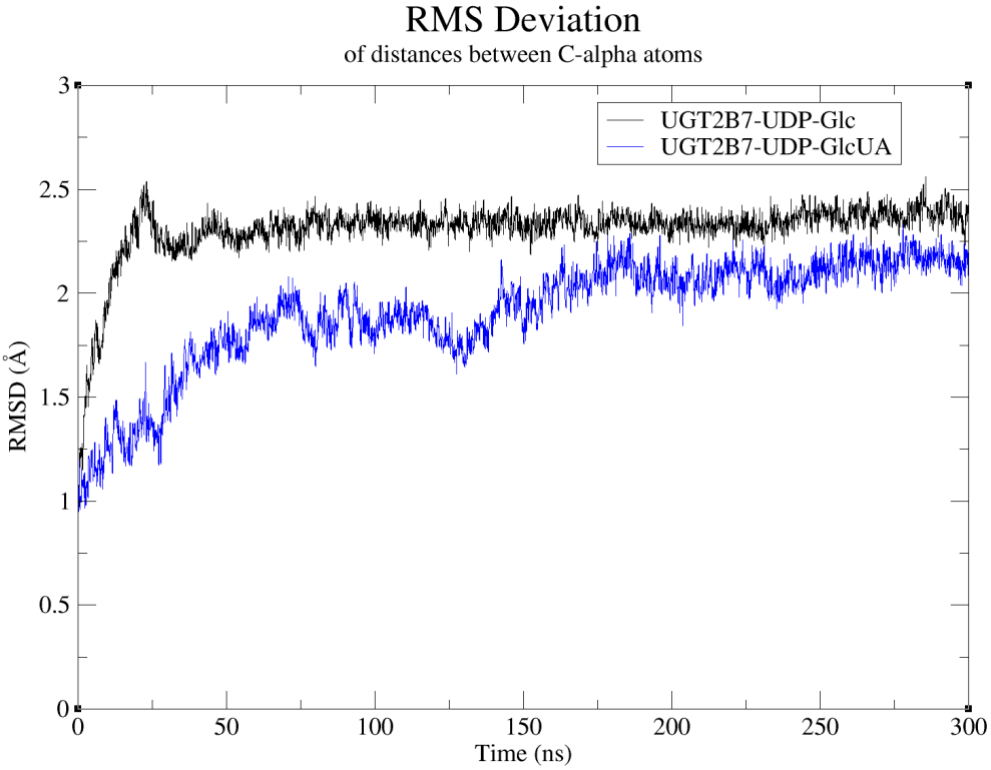

Figure S2 Root mean squared deviation (rmsd) of the Cα atoms of UGT2B7 with bound UDP-Glc (black) and UDP-GlcUA (blue).

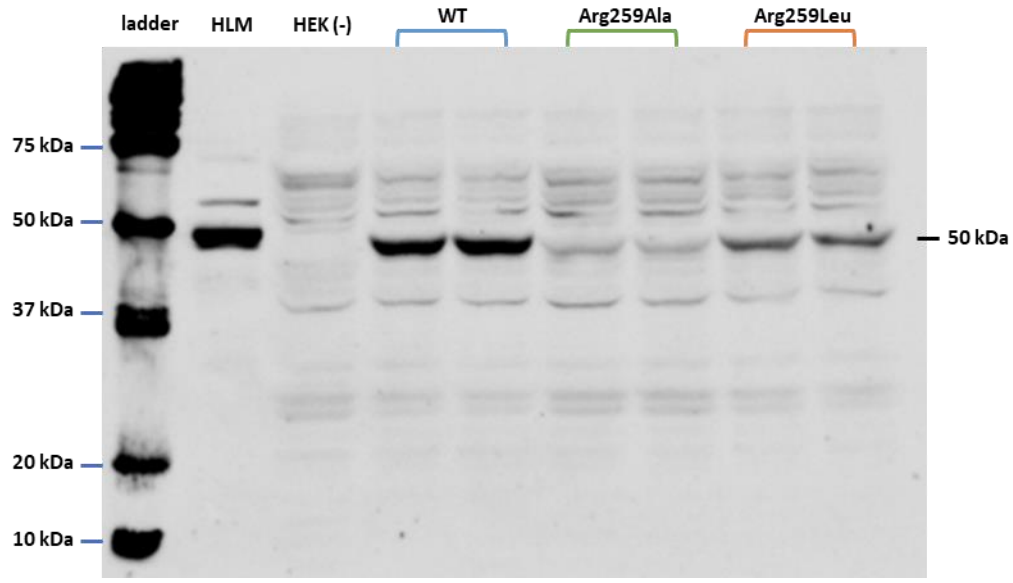

Figure S3 Immunoblots of wild-type and mutant UGT2B7 proteins showing relative expression from stable transfection in HEK293T cells. Lysate protein preparations (50µg) were resolved by SDS-PAGE, blotted to nitrocellulose, and probed with anti-human UGT2B7 antisera. Immuno-reactive bands are present at 50 kDa. Lanes 1 (positive; HLM) and 2 (negative; untransfected HEK293T) contain control samples.

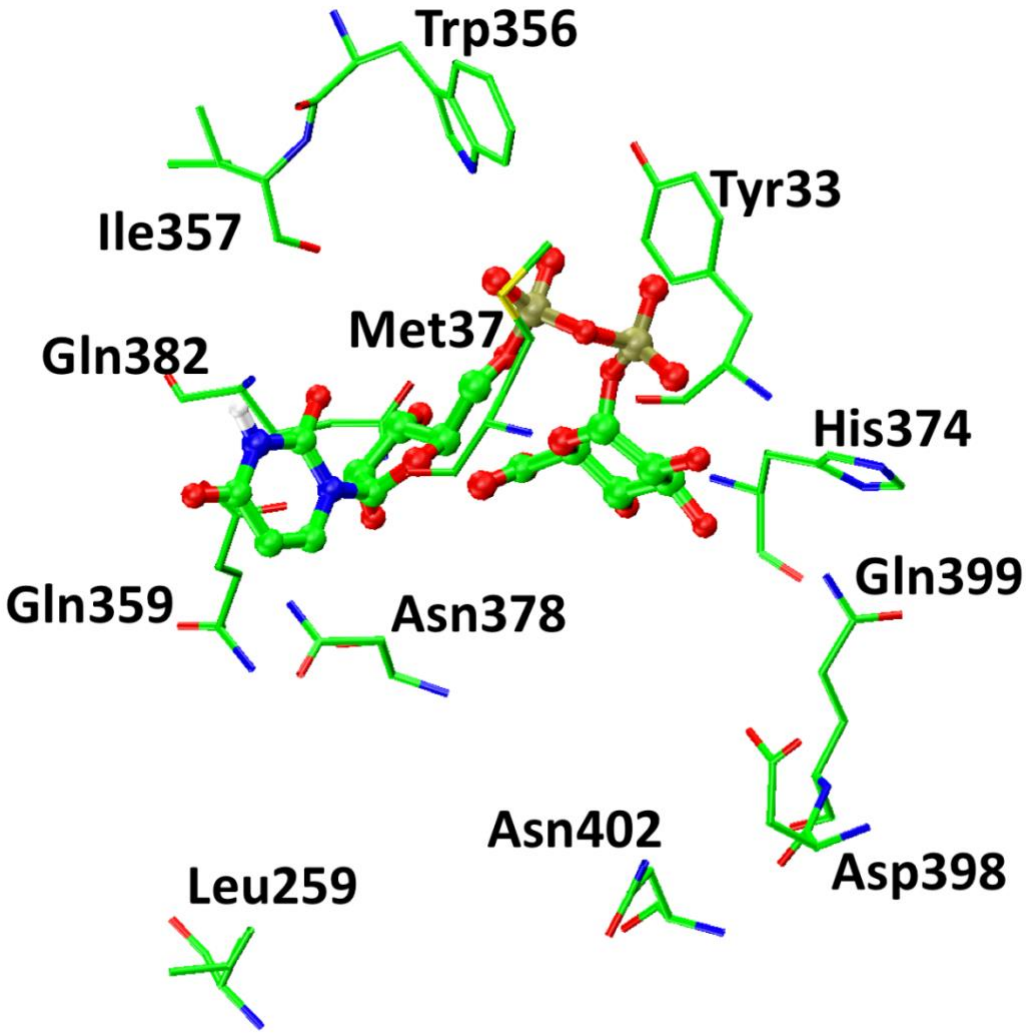

Figure S4 Snapshot from MD simulations of UDP-GlcUA (ball and sticks) in the UGT2B7 Arg259Leu mutant. Key residues (sticks) within the binding site are displayed. C, O, N, S and P are shown in green, red, blue, yellow, and orange, respectively.

Supplemental Material Movie Stable interaction (H-bonding and salt-bridge) between Arg259 of the UGT2B7 and UDP-GlcUA.